,

Commissioning of the electron injector for the AWAKE experiment

S.-Y. Kim[*] and M. Chung[†]

*Department of Physics, Ulsan National Institute of
Science and Technology, Ulsan 44919, Republic of Korea*

M. Dayyani

Institute for Research in Fundamental Sciences, 19395-5531, Tehran, Iran

S. Doebert[‡] and S. Gessner, I. Gorgisyan, S. Mazzoni, M. Turner

BE Department, CERN, Geneva 1211, Switzerland

J. T. Moody

Max Planck Institute for Physics, 80805 Munich, Germany

R. Apsimon, G. Burt

*Lancaster University, LA1 4YW Lancaster,
United Kingdom, Cockcroft Institute,
WA4 4AD Warrington, United Kingdom*

O. Apsimon, B. Williamson

*Manchester University, M13 9PL Manchester,
United Kingdom, Cockcroft Institute,
WA4 4AD Warrington, United Kingdom*

Abstract

The Advanced Wakefield Experiment (AWAKE) at CERN is the first proton beam-driven plasma wakefield acceleration experiment. The main goal of AWAKE RUN 1 was to demonstrate the seeded proton beam self-modulation (SSM), and the electron witness beam acceleration in the plasma wakefield. For the AWAKE experiment a 10-meter-long Rubidium-Vapor cell together with the high-power laser for ionization has been used to generate the plasma. The plasma wakefield is driven by a 400 GeV/c Proton beam extracted from the Super Proton Synchrotron (SPS) which is self-modulated, a mechanism seeded by the lionization laser. The electron witness beam used to probe the wakefields is generated from a S-band RF photo-cathode gun and then accelerated by a booster structure up to energies between 16 and 20 MeV. In the first run of the AWAKE experiment, it has been measured that the energy gain after the plasma cell can reach up to 2 GeV, and the SSM mechanism of the proton beam has been verified. In this paper, we present the details of the AWAKE electron injector used for the electron acceleration experiments. A comparison of the measured electron beam parameters such as beam size, energy and normalized emittance with the simulation results will be shown.

---

*Electronic address: sykim12@unist.ac.kr

†Electronic address: mchung@unist.ac.kr

‡Electronic address: steffen.doebert@cern.ch

I. INTRODUCTION TO AWAKE

The Advanced Wakefield Experiment (AWAKE) at CERN studies electron beam acceleration in proton beam-driven plasma wakefields [1, 2]. The proton beam driver has a momentum of 400 GeV/c, a bunch length of 6-12 cm (RMS), and a transverse beam size of 0.2 mm (RMS). The plasma is generated in a 10-meter-long heated Rubidium-Vapor source that can reach plasma densities of the order of $1 \times 10^{14} \sim 1 \times 10^{15}$ $/cm^3$. The ionization laser has an energy of 450 mJ and a pulse length of 120 fs (FWHM) allowing full ionization of a plasma channel with a radius of 1 mm. The laser pulse and the proton beam co-propagate through the vapor source to create the plasma and seed the self modulation within the long proton bunch. The maximum accelerating gradient of the plasma wakefield [3] $E_{max} = m_e w_{pe} c/e$ is determined by the plasma electron density n_e where m_e is the electron mass, $w_{pe} = \sqrt{n_e e^2 / m_e \epsilon_0}$ is the plasma frequency, ϵ_0 the vacuum permittivity, c the speed of light, and e the electron charge, respectively. In the case of AWAKE, the nominal plasma density is 7×10^{14} $/cm^3$, and the maximum accelerating gradient is therefore expected to be on the order of GV/m.

Particular to AWAKE, an important condition for the generation of high plasma wakefields is the Seeded Self-Modulation (SSM) of the proton beam [4, 5]. In the linear plasma wakefield theory the optimal condition to drive plasma wakefields is $k_p \sigma_z \cong \sqrt{2}$ where k_p is the plasma wavenumber defined by w_{pe}/c, and σ_z is the RMS bunch length of the drive beam [6]. Therefore, the initial proton beam extracted from the Super Proton Synchrotron (SPS) does not satisfy the condition to generate high-gradient wakefields due to its long bunch length. However, once the long proton bunch has propagated for a distance in the plasma, it splits into micro-bunches which have a length corresponding to the plasma wavelength, meeting the condition for driving the high-gradient plasma wakefield [7]. The self-modulation of the proton beam is reliably seeded by the front of the ionization laser which is placed in the center of the proton beam, then the self-modulation of the proton beam density starts from this point enabling phase stable wakefields.

In the first run of the AWAKE experiment to demonstrate electron beam acceleration through the plasma wakefields, an electron injector that consists of a S-band RF photocathode gun, and a traveling wave booster structure has been used to produce electron beams with an energy of 16-20 MeV [8, 9]. The electron beam is then passing through an electron

transfer line, and injected into the plasma cell co-propagating with the proton beam and the ionization laser [10]. An energy gain of the electron beam in the 10 m plasma source of up to 2 GeV [11] has been demonstrated experimentally. In addition, the SSM phenomenon has been successfully observed and studied by direct measurement of the modulated proton bunch using streak cameras, and by indirect measurement of the proton beam divergence due to the transverse wakefield [12, 13]. A schematic of the AWAKE experiment can be seen in fig 1.
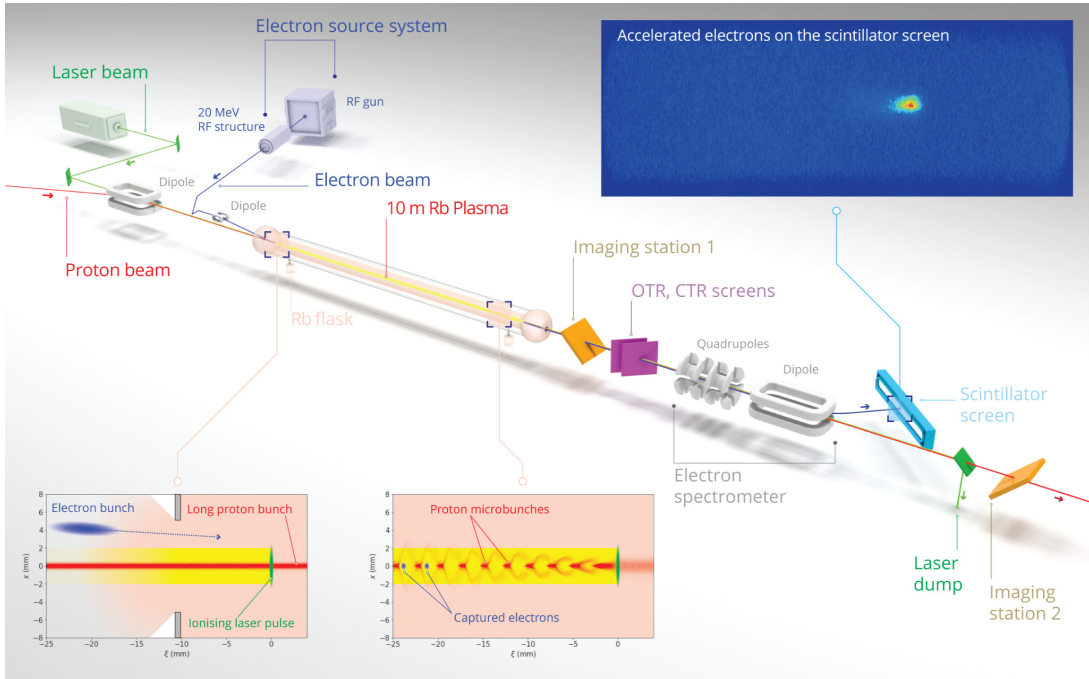
FIG. 1: Schematic of the AWAKE experiment at CERN. The upper right corner shows an example of a beam spot as observed in the spectrometer. The inserts in the lower left corner illustrate the injection conditions and the process of seeded self modulation.

In this paper, we present the details of the electron injector used for the acceleration experiment in Section II. Commissioning results such as transverse beam distributions on screens and the beam emittance measurements using pepper-pot and quadrupole scan methods will be shown in the Section III. A careful comparison of the measurements with the simulation results in order to demonstrate the operating condition of the electron injector will be presented in Section IV. Finally, the results of the commissioning will be concluded in the Section V.

II. DESIGN AND CONSTRUCTION OF THE INJECTOR

An electron injector providing adequate beam quality to demonstrate the first proton driven plasma wakefield acceleration experiment was designed and constructed within the AWAKE collaboration. The original target parameters for the injector were an energy of 16 MeV, a bunch charge of 200 pC, an energy spread below 1%, a bunch length of 4 ps and an emittance of 2 mm mrad. The small emittance was needed to provide an adequate spot size matching the plasma parameters at the injection point. To achieve these parameters an RF photo-injector was chosen using a 3 GHz, 2.5-cell RF-gun and a one-meter-long booster structure. The RF-gun including a load-lock system was available at CERN [14], while the booster structure was newly developed for this purpose [8]. The load-lock system allows to use Cs_2Te cathodes fabricated at CERN with a quantum efficiency of Qe $\sim 10^{-2}$. The laser beam was derived from the main Ti-Sa laser used to ionize and seed the proton beam self-modulation. Consequently, an adequate timing synchronization could be achieved. A small fraction of the initial laser power is frequency tripled to a wavelength of 262 nm and sent with an off-axis mirror on the cathode. The UV-beamline allows to vary the spot size and energy on the cathode as well as the bunch length since the IR-laser beam has to be compressed before the UV conversion [15]. The RF-gun accelerated the electron bunches to an energy of 5.5 MeV followed by the booster which can add up to 16 MeV. A single klystron is used to power the gun and the booster structure. A high power wave-guide attenuator and phase-shifter allow for individual phasing and powering of the two structures. A particular challenge for the design and construction was the severe space constraints in the AWAKE experiment. The complete injector has a total length of only 5 m before the beam transport towards the plasma cell starts. The injector is equipped with a number of beam diagnostics as described in more detail in the next section.

III. BEAM COMMISSIONING RESULTS

Figure 2 shows a schematic view of the electron injector indicating in particular the locations of focusing and beam diagnostic elements used in this section. The electron injector consists of an S-band RF photocathode gun and booster structure. The main solenoid and the corresponding bucking coil are placed around the RF gun to control the beam focusing
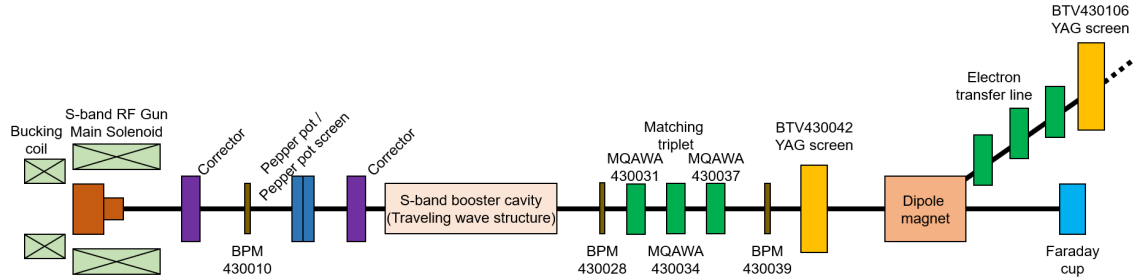
FIG. 2: Schematic electron injector layout emphasizing the location of magnets and diagnostics mentioned throughout the paper.

and emittance compensation. Corrector magnets are used to correct the beam trajectory which can be measured with several strip-line BPM's [16]. A pepper-pot beam diagnostic instrument is used to measure the beam emittance out of the RF-gun, the corresponding screen behind the retractable pepper-pot also allows imaging of the transverse distribution of the beam. A quadrupole triplet behind the booster structure is used to match the beam for further beam transportation and for the emittance measurements using the quadrupole scan method at higher energies. A YAG screen (BTV430042) is used for the measurement of the transverse beam distribution. The electron beam charge at the end of the injector is measured in a Faraday-Cup with high precision. The first dipole magnet of the following transport line together with a second screen also serves as a spectrometer to measure the beam energy and energy spread. During the commissioning, as many beam parameters as possible were measured to be used as input parameters for simulations.

First, the initial laser pulse distribution which produces the electron bunch by illuminating the cathode has been measured using the so-called virtual cathode camera. This camera images a fraction of the laser beam in similar imaging conditions as the laser pulse sent to the cathode. The laser energy can be varied with Optical Density (OD) filters to adjust the final beam charge. The beam charge during the commissioning measurements reported here was measured to be 140 ± 10 pC. The initial transverse distribution of the laser is shown in Fig. 3. Figure 3 (a) shows the case without OD filter to enhance the UV imaging. The RMS transverse beam size can be determined to be $\sigma_x = 0.33$ mm in the horizontal plane, and $\sigma_y = 0.34$ mm in the vertical plane respectively. In the experiment, however, an OD filter was used to reduce the beam charge, which results unfortunately in a poorer quality image of the virtual cathode as can be seen in Fig. 3 (b). The transverse size of the laser obtained

by analyzing this image appears slightly reduced due to the cut-off of the laser energy, and we obtain σ_x and σ_y are 0.27 mm. The smaller values were used for the particle tracking simulations later on. The bunch length of the electron beam was not measured during the experiment. Older measurements of the UV laser beam suggested a laser pulse length of σ_z = 2.208 ps (FWHM 5.2 ps).
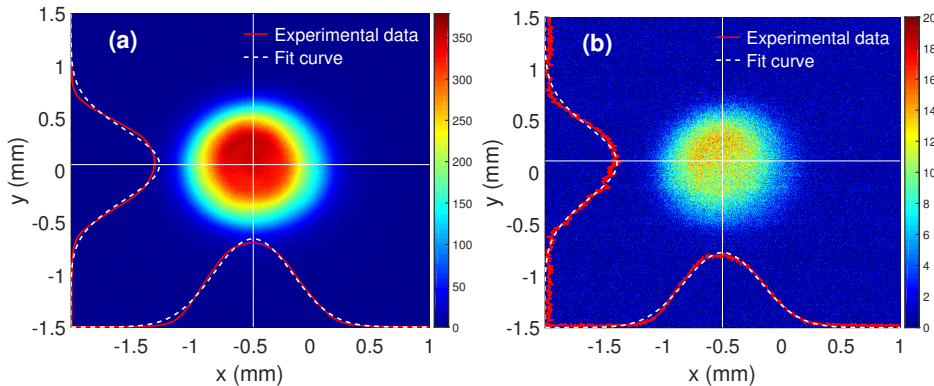
FIG. 3: Initial transverse distribution of the laser at the cathode without OD filter (a), and with OD filter (b).

The energy of the electron beam out of the RF gun has been calculated by measuring the position of the beam at the pepper-pot screen while scanning the first corrector magnet since no real spectrometer is available after the gun. The electron beam momentum out of the RF-gun was determined to be 5.8 MeV/c, which corresponds to a nominal energy of 5.31 MeV. However, since this measurement has a much lower quality compared to a real spectrometer magnet we estimate the error of the electron beam energy calculation to be about 10%. The energy of the electron beam after the traveling wave structure has been measured using the first dipole magnet in a proper spectrometer setup. The momentum of the electron beam after acceleration was determined to be 18.5 MeV/c with an error of 0.3%. To optimize the operating conditions of the electron injector during commissioning, scans of the main solenoid around the RF-gun responsible for emittance compensation have been performed. Beam sizes and emittances have been measured before and after the booster structure as a function of the solenoid current. First, the transverse beam size of the electron beam was measured on the pepper-pot screen. Figure 4 (a) depicts the beam size and normalized emittance as a function of the solenoid current. Minimum beam sizes σ_x and σ_y at the pepper-pot screen are 0.47 mm, and 0.38 mm for a solenoid current of 185 A. We found

during the commissioning that it was very difficult to get reliable and reproducible emittance measurements with our pepper-pot setup. The cause of that is still under investigation. At this point, we tend to not believe these measurements. We will come back to that issue in the simulation section.

In addition to the measurement at the pepper pot screen, beam size and the normalized emittance after the traveling wave structure have been measured. This time a well established quadrupole scanning method was used since the beam is no longer space charge dominated. The beam size has been measured at the BTV430042 screen, while the normalized emittance was determined from a quadrupole scan by varying the magnetic field of the center quadrupole of the triplet (MQAWA430034). Figure 4 (b) shows the beam size at the screen (BTV430042), and the normalized emittance as a function of the solenoid current. The minimum beam size was found at the solenoid current of 175 A: σ_x is 0.30 mm, and σ_y is 0.29 mm. The minimum normalized emittance however was found at a solenoid current of 185 A, which are 1.01 mm mrad in the horizontal plane, and 1.06 mm mrad in the vertical plane, respectively.
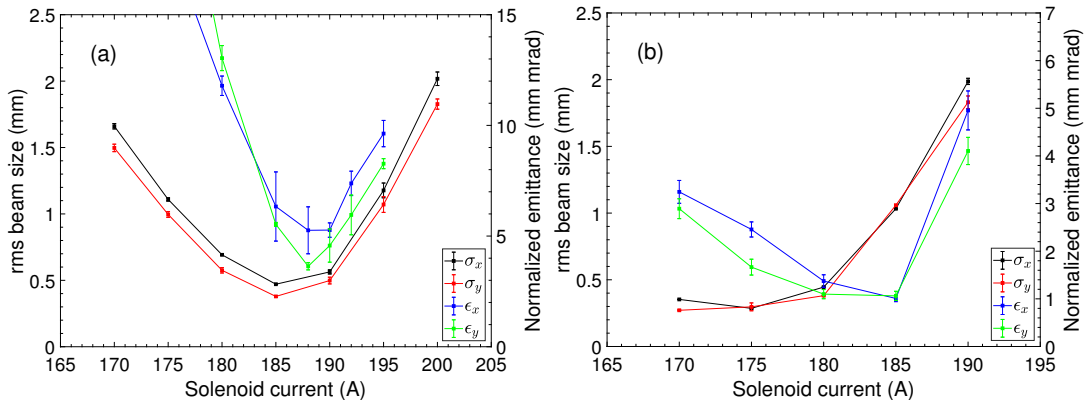
FIG. 4: Measured transverse beam size and normalized emittance of the electron beam at the pepper-pot (a), and BTV 430042 screen (b).

In the next section, we will show a comparative analysis of experimental measurements with the results obtained from simulations.

IV. COMPARISON WITH SIMULATIONS

In order to compare measured beam parameters with the simulation results, particle tracking has been performed mainly using the ASTRA [17] code. The cathode material used in AWAKE is Cs_2Te, and characteristic parameters of the electron beam emitted from the cathode such as thermal emittance, momentum distribution can be defined as the Fermi-Dirac distribution [18, 19]. In ASTRA, the momentum distribution, and thermal emittance of the initial beam at the cathode are defined as follows [20].

$$\sigma_{p_x} = \sigma_{p_y} = \sqrt{\frac{E_{photon} - \phi_{eff}}{3m_ec^2}}, \tag{1}$$

$$\sigma_E = \frac{E_{photon} - \phi_{eff}}{3\sqrt{2}}, \tag{2}$$

$$\epsilon_{x,y} = \sigma_{x,y}\sqrt{\frac{E_{photon} - \phi_{eff}}{3m_ec^2}}, \tag{3}$$

where $\sigma_{p_{x,y}}$ is the RMS value of the transverse momentum, E_{photon} is the photon energy of the laser, ϕ_{eff} is the effective work function of the cathode material, σ_E is the energy spread, and $\epsilon_{x,y}$ is the thermal emittance, respectively.

Through above equations and Ref. [19], the transverse momentum and energy spread are determined only by the photon energy of the laser and the work function of the cathode material, regardless of the spatial distribution type of the laser. Based on the fact that the momentum distribution is determined by E_{photon} and ϕ_{eff} irrespective of the laser shape, the initial beam distribution measured at the cathode (see previous section), was used as an input to the simulation. As can be seen in Fig. 3 (b), the distribution is not fully symmetric. In order to perform the simulations we converted the measured image into an transverse input distribution suitable for simulations. For the longitudinal components, a distribution generated by ASTRA was used assuming a Gaussian laser pulse shape. For the simulations, since we do not have a real bunch length measurement, we studied three values, the 2.2 ps as indicated by older UV laser measurements and shorter beams with 1.0 ps, and 1.5 ps bunch length for comparison.

The RF fields of the RF gun are overlaid with the magnetic fields of the solenoids. The maximum accelerating gradient has been set to be 79.6 MV/m to obtain the measured

beam energy of 5.3 MeV out of the RF gun. At 1.6 m, a traveling wave structure (booster structure) has been placed to increase the beam energy to match the measured value of 18.1 MeV, therefore its accelerating gradient is 17.8 MV/m. In the ASTRA simulation a full 3D field map of the booster structure obtained from CST has been used, while the field map of the RF gun is determined by the 1D axial electric field due to a lack of 3D data. The phase of the gun has been checked to achieve the maximum energy gain, corresponding nominally to the smallest emittance as well. Therefore the beam launch phase is approximately 30° off crest in the simulations. In the experiment, we tried to minimize the emittance varying the phase of the gun and solenoid around the nominal working point. The traveling wave booster structure was set to on-crest acceleration as optimised for maximum energy in the experiment.
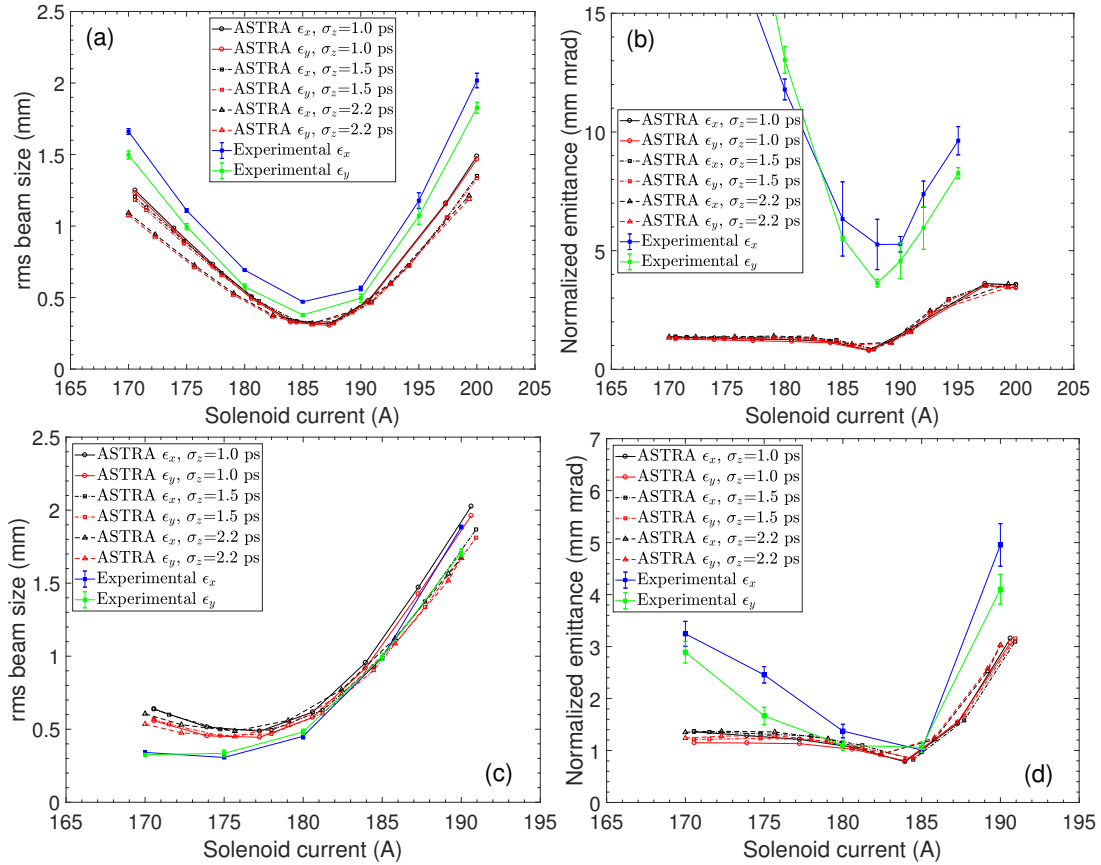
FIG. 5: Transverse beam size, and normalized emittance obtained from ASTRA simulation at the pepper-pot screen (a, b), and BTV430042 screen (c, d) without misalignement.

Solenoid scans have been simulated with bunch lengths of 1 ps, 1.5 ps and 2.2 ps. The simulation results together with the measured data are shown in Fig. 5, upper plots for the

pepper-pot screen and the lower plots for the BTV 430042 screen. In this case, misalignment of the RF structure, and solenoid magnet have not been considered. One can see that the slopes of the beam size scans match better with shorter bunch length on both screens. This results indicate that the bunch length might have been shorter than 2.2 ps as indicated by older UV measurements. At the pepper-pot screen, the minimum beam sizes σ_x and σ_y for the case of 1 ps bunch length are 0.32 mm, 0.31 mm, and the minimum values of the normalized emittance are 0.80 mm mrad in the horizontal plane, and 0.78 mm mrad in the vertical plane. In addition, the minimum beam sizes σ_x and σ_y at the BTV430042 screen are 0.48 mm and 0.44 mm, and the minimum values of the normalized emittance are very similar to the values at the pepper-pot screen. However, the shape of the scan for the emittance measurements does not correspond well to the simulations. The emittance determination using the pepper-pot data seems to fail since the larger measured values do not agree neither with simulations nor with the quadrupole scan measurements which seem to match the simulations at least for the minimum values. The emittance values measured using the pepper-pot device and method seem not to match at all the expectations from simulations while the measurements further downstream of the beam line using the quadrupole scan method seem to match well at least for the region of the minimum. Therefore at this point we concluded that the pepper-pot results are likely not reliable. The reason for this is still under investigation, there are hints that the location and dimensions of our device are not optimal [21].

During the experiments, the machine operation and in particular the beam alignment were optimized for the minimum emittance values at 185 A since these beams have been used for the plasma wakefield acceleration experiments. The alignment of the beam was not corrected during the scan. Therefore, we suspect some misalignment of the beam due to steering of the solenoid magnet as a cause for the particular shape of the emittance measurements. Particle tracking simulations have been used again to study possible offsets of the booster structure and the solenoids since we had some experimental hints from beam trajectory data that this might have been the case.

Various offsets of the main solenoid and the booster structure have been studied using ASTRA with 3D space charge calculations and a 3D field map for the booster structure. It turned out that the measurements are best described assuming a relatively big offset of the booster structure only. Figure 6 shows the simulation results obtained for a -4.5 mm offset
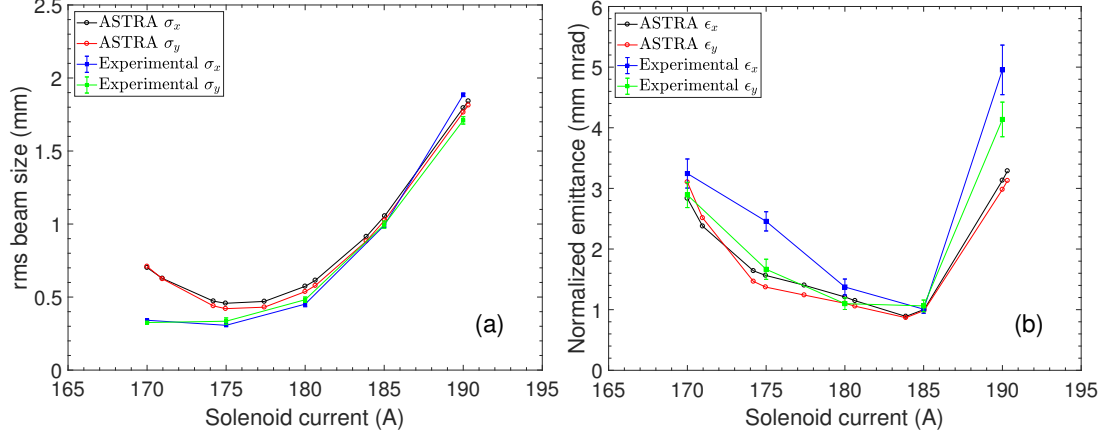
FIG. 6: Comparison of the transverse beam size (a) and normalized emittance (b) at BTV430042 screen taking into account a misalignment of the booster structure.

at the entrance of the booster structure in comparison with the experimental data. In this simulation, 1.5 ps bunch length was used. Both the emittance and the spot size show good qualitative agreements for these misalignment assumptions.
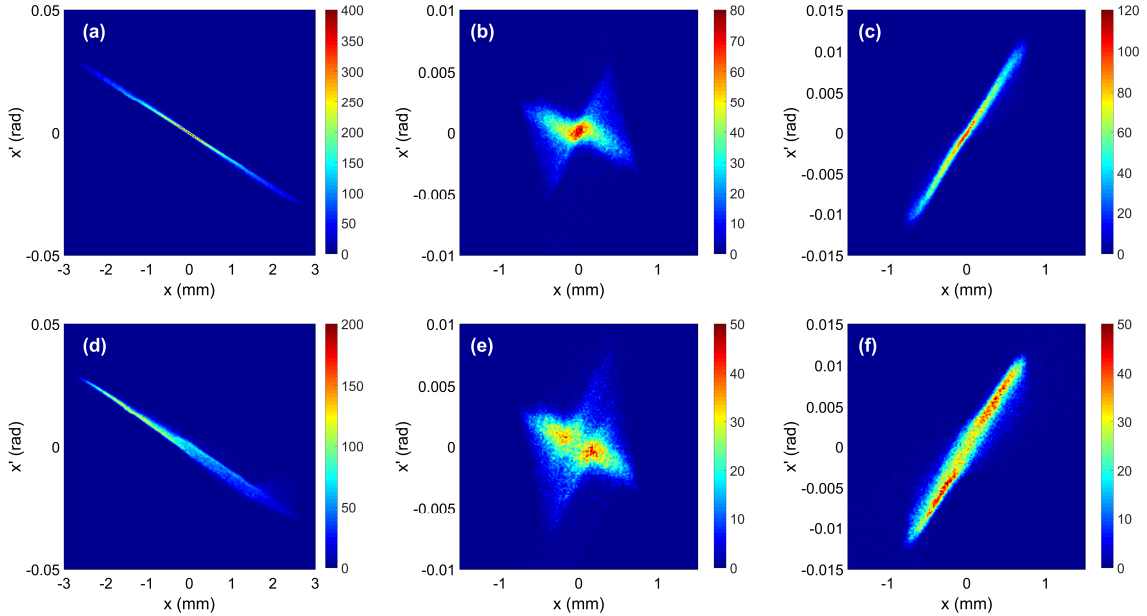
FIG. 7: Horizontal phase space of the beam at the input coupler section. Top: on-axis simulation, bottom: off-axis simulation with -4.5 mm booster structure offset. Solenoid current: (a, d) 170 A, (b, e) 185 A, (c, f) 190 A.

The main reason for the emittance growth seen in the simulations is an RF kick within

the input coupler of the booster structure due to its not perfectly compensated RF fields. The beam size is large at this location for low and high solenoid fields (170 A and 190 A) which leads to a sampling of this asymmetric fields across the beam size. Phase space distortion due to the asymmetric field is illustrated in Figure 7 where the top row shows the horizontal phase space at the input coupler of the booster structure obtained from on-axis simulation, while the bottom row images are with the booster structure offset. One can see that the momentum distribution of the on-axis case is concentrated in the center. In the case with a large beam offset, simulation results show that the momentum distribution is distorted with respect to the core, which leads to the emittance growth. However, for well focused beams at the entrance of the booster (solenoid currents of 180 and 185 A), the effect is much smaller and the emittance growth is not significant.

In a second beam commissioning campaign the misalignment of the beam in the booster structure and the question of the not well known bunch length was addressed. The original misalignment of the solenoids could not be solved therefore we corrected the beam at the entrance of the booster structure for each solenoid setting using a pair of corrector magnets when taking data. In addition, since the UV pulse shape and length were not clearly determined during the last measurement, UV pulse measurements using streak camera were performed again. Unfortunately, it was not possible to get reliable data from direct bunch length measurements using light from an OTR screen on the streak camera. The intensity arriving at the streak camera was simply not high enough.
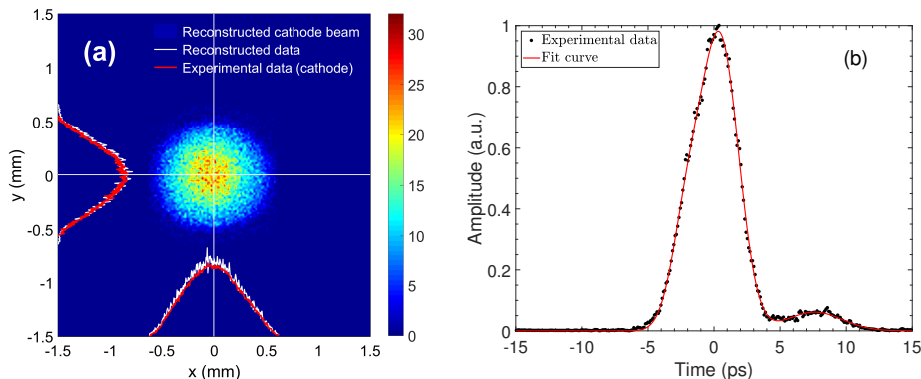
FIG. 8: Initial transverse beam distribution at the cathode (a), and longitudinal profile of the UV laser pulse (b). Intensity of the UV laser is normalized.

The transverse beam distribution and charge of the beam were slightly different from the

13

first campaign therefore the following inputs were used for the simulations. Figure 8 shows the measured transverse beam distribution at the cathode and the measured longitudinal profile of the UV laser pulse. The initial beam size is slightly changed compared to Fig. 3 (b). beam sizes σ_x and σ_y is 0.25 mm. The measured beam charge at the Faraday cup was 150 pC. In the case of the UV measurement, it has been confirmed that the RMS UV pulse length was 1.5 ps. In addition one can see that there is secondary pulse behind main pulse, but it should be negligible since the amplitude is very small compared to the main pulse. This after-pulse was not taken into account in the simulations. Even though the simulation results with 1.5 ps bunch length is not perfectly matched with the experimental data indicated in Fig. 5, it has been confirmed that the measured bunch length is significantly shorter than assumed previously.

Using the new measured inputs ASTRA simulations have been performed again. The booster structure gradient has been slightly changed to obtain the experimentally measured 18.8 MeV/c momentum value in the simulation. This time we obtained a good agreement between simulations and measurements confirming the assumptions concluded from the analysis of the first measurement campaign. The measured emittance values obtained from quadrupole scans and the simulation results are compared in Fig. 9. In addition the overall emittance of the beam has been reduced due to a better and more careful setup of the beam.
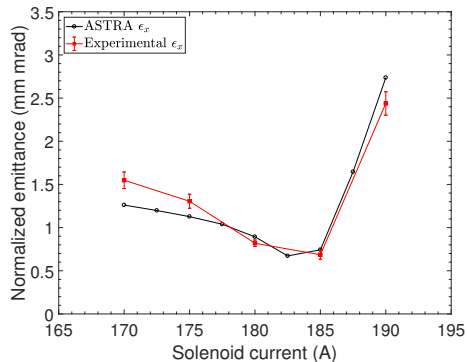
FIG. 9: Horizontal normalized emittance measured at the BTV 430042 screen compared to simulations.

V. CONCLUSIONS

The probe beam electron injector for the AWAKE experiment has been successfully constructed and commissioned. It enabled the succesful demonstration of the first ever proton driven plasma wakefield experiments. Despite the time constraints of beam delivery for acceleration experiments, systematic beam commissioning measurements were successfully performed with the electron injector. These measurements were compared with intensive beam dynamics modeling using ASTRA. A maximum of measured input parameters was used to reproduce the experimental results. There was good overall agreement giving us confidence in our injector model. In order to improve the agreement even further two main parameters were identified, a potentially large misalignment in the booster structure and a tendency for a shorter initial bunch length as originally anticipated. Recent UV pulse measurement confirmed that the actual measured pulse length was shorter as expected by the simulations. Correcting the alignment of the beam through the booster structure for each solenoid setting improved the emittance and resulted in a good agreement compared to simulations assuming an on-axis beam. The next step for AWAKE is to inject a very short bunch of 200 fs, with a matched beta-function and bunch charge to load the wakefield into the plasma. The goal will be to demonstrate emittance preservation and a low energy spread at the end of the plasma acceleration. This challenging task requires a new injector which is currently under design. The good agreement between simulations and measurements for the current injector gives us confidence for the future work.

---

[1] A. Caldwell, E. Adli, L. Amorim, R. Apsimon, T. Argyropoulos, R. Assmann, A.-M. Bachmann, F. Batsch, J. Bauche, V. B. Olsen, et al., Nuclear Instruments and Methods in Physics Research Section A: Accelerators, Spectrometers, Detectors and Associated Equipment **829**, 3 (2016).

[2] E. Gschwendtner, CERN Yellow Reports **1**, 271 (2016).

[3] J. M. Dawson, Physical Review **113**, 383 (1959).

[4] P. Muggli, E. Adli, R. Apsimon, F. Asmus, R. Baartman, A. Bachmann, M. B. Marin, F. Batsch, J. Bauche, V. B. Olsen, et al., Plasma Physics and Controlled Fusion **60**, 014046 (2017).

[5] M. Huther and P. Muggli, Nuclear Instruments and Methods in Physics Research Section A: Accelerators, Spectrometers, Detectors and Associated Equipment **909**, 67 (2018).

[6] W. Lu, C. Huang, M. Zhou, W. Mori, and T. Katsouleas, Physics of plasmas **12**, 063101 (2005).

[7] K. Lotov, Physics of Plasmas **22**, 103110 (2015).

[8] O. Mete, G. Xia, R. Apsimon, G. Burt, S. Doebert, R. Fiorito, and C. Welsch, arXiv preprint arXiv:1505.02621 (2015).

[9] K. Pepitone, S. Doebert, R. Apsimon, J. Bauche, M. Bernardini, C. Bracco, G. Burt, A. Chauchet, E. Chevallay, N. Chritin, et al., Nuclear Instruments and Methods in Physics Research Section A: Accelerators, Spectrometers, Detectors and Associated Equipment **909**, 102 (2018).

[10] M. Turner, C. Bracco, S. Gessner, B. Goddard, E. Gschwendtner, P. Muggli, F. P. Asmus, F. Velotti, and L. Verra, in *2018 IEEE Advanced Accelerator Concepts Workshop (AAC)* (IEEE, 2018), pp. 1–4.

[11] E. Adli, A. Ahuja, O. Apsimon, R. Apsimon, A.-M. Bachmann, D. Barrientos, F. Batsch, J. Bauche, V. B. Olsen, M. Bernardini, et al., Nature **561**, 363 (2018).

[12] M. Turner, E. Adli, A. Ahuja, O. Apsimon, R. Apsimon, A.-M. Bachmann, M. B. Marin, D. Barrientos, F. Batsch, J. Batkiewicz, et al., Physical review letters **122**, 054801 (2019).

[13] E. Adli, A. Ahuja, O. Apsimon, R. Apsimon, A.-M. Bachmann, D. Barrientos, M. Barros, J. Batkiewicz, F. Batsch, J. Bauche, et al., Physical review letters **122**, 054802 (2019).

[14] O. Mete and et al., Physical Review ST Accelerators and Beams **15**, 022803 (2012).

[15] V. Fedosseev, F. Batsch, C. Capelli, E. Chevallay, N. Chritin, S. Döbert, T. Feniet, F. Friebel, P. Gander, E. Granados, et al., in *10th Int. Partile Accelerator Conf.(IPAC'19), Melbourne, Australia, 19-24 May 2019* (JACOW Publishing, Geneva, Switzerland, 2019), pp. 3709–3712.

[16] S. Liu, V. Verzilov, W. Farabolini, S. Doebert, and S. Schmidt, Proc. International Conference on Technology and Instrumentation in Particle Physics, Beijing, China (2017).

[17] K. Floettmann, *A space charge tracking algorithm*, URL `http://www.desy.de/~mpyflo/`.

[18] K. Flöttmann, Tech. Rep., SCAN-9708052 (1997).

[19] D. H. Dowell and J. F. Schmerge, Physical Review Special Topics-Accelerators and Beams **12**, 074201 (2009).

[20] K. Flöttmann et al., ASTRA Manual (2011).

[21] O. Apsimon, B. Williamson, and G. Xia, Nuclear Instruments and Methods in Physics Research Section A: Accelerators, Spectrometers, Detectors and Associated Equipment **943**, 162485 (2019).